Available online at www.sciencedirect.com
SCIENCE DIRECT
ELSEVIER
Colloids and Surfaces A: Physicochem. Eng. Aspects xxx (2005) xxx–xxx
COLLOIDS AND SURFACES A
www.elsevier.com/locate/colsurfa

Towards the abatement of environmental mercury pollution: An electrochemical characterization

B.F. Giannetti [a,*], W.A. Moreira [b], S.H. Bonilla [a], C.M.V.B. Almeida [a], T. Rabóczkay [c]

[a] *Instituto de Ciências Exatas e Tecnologia da Universidade Paulista, LaFTA-Laboratório de Fisicoquímica Teórica e Aplicada, R. Dr. Bacelar 1212, 04026-002 São Paulo, SP, Brazil*
[b] *Faculdade de São Bernardo do Campo, R. Américo Brasiliense 449, 09715-020 São Bernardo do Campo, SP, Brazil*
[c] *Instituto de Química da Universidade de São Paulo, PO BOX 26077, 05599-970 São Paulo, SP, Brazil*

Received 5 September 2005; accepted 28 October 2005

Abstract

Electrochemical experiments in acetic acid–acetate buffer (pH 4.5) are conducted in order to understand metallic and ionic mercury adsorption processes on the pyrite surface. The nature as well as the extent of the spontaneous interaction between pyrite and mercuric ions was evaluated. The spontaneous reduction of mercury species onto pyrite surface was confirmed. These results represent a first step for the use of mining wastes rich in pyrite for mercury pollution abatement.

Keywords: Electrochemistry; Mercury abatement; Mercury pollution; Pyrite; Spontaneous adsorption

1. Introduction

Environmental pollution due to the discharge of heavy metals has motivated extensive research work dealing with the understanding of the mechanisms controlling speciation, availability and mobility of these species in natural systems. The resulting knowledge gathered by this research offers a starting point to propose solutions to reduce impacts caused by heavy metals release in the environment.

Elemental mercury discharged into natural aquatic systems is retained in lake and river sediments. Under anaerobic conditions, the elemental mercury is converted into alkyl mercury species by the action of micro-organisms [1]. Both organic and inorganic mercury species are toxic. The literature cites fatal incidents due to methyl mercury ingestion in Minamata [2] and Irak [3]. More recently, the death of a researcher as a consequence of skin contact with $(CH_3)_2Hg$ was described [4].

Several works concerning heavy metal adsorption on different adsorbent surfaces are found in literature. An extensive revision of non-conventional strategies for heavy metal adsorption has been recently published [5]. There, the concept of eco-technologies is discussed and integration between industries is emphasised, with respect to their waste treatment. A real example about adsorption of chromium on pyrite surfaces, by-products from tannery and from mining industries, respectively, is provided [5].

Among the works dealing with heavy metal adsorption, it is worthy of highlight, those of Kinniburg et al. [6], Balistrieri and Murray [7], and Forbes et al. [8] using goethite; Loganathan and Burau [9] employing hydrous oxide gels; Farrah et al. [10] with manganese oxides; Hara et al. [11] using synthetic pumice; and Baba et al. [12] using special chelating resins. The use of iron sulfide minerals as adsorbent substrates for mercury is found in a few works [13–17]. Brown et al. [13] present a study comparing the performance of iron sulfides and oxides as adsorbents for mercury. The correlation between the capacity of sulfide mineral adsorption and pH is also discussed. The study also confirms that both pyrite and pyrrhotite are excellent adsorbent materials for heavy metals. According to the authors, mercury ions present a great affinity for sulfide surfaces. The lower value of the solubility constant of mercury sulfide ($K_s = 10^{-52}$) confirms this fact.

The studies regarding mercury adsorption on sulfide minerals are mainly devoted to the development of a methodology to

* Corresponding author.
E-mail address: biafgian@unip.br (B.F. Giannetti).

0927-7757/$ – see front matter © 2005 Elsevier B.V. All rights reserved.
doi:10.1016/j.colsurfa.2005.10.052

remove this pollutant from the environment. Jean and Bancroft [14] and Hiland et al. [15] made the attempt to characterize the mineral surface resulted from the interaction with heavy metals by X-ray photoelectronic and Auger spectroscopy. These techniques failed in the species identification, and even the combination of both atomic absorption and X-ray photoelectronic spectroscopy techniques [13,14] was not able to identify the mercury species involved.

Hiland et al. [15] affirm that more than a species is present on the mineral surface, and until now the nature of the species formed as a consequence of the interaction between sulfide minerals and Hg(II) solutions is unknown.

On the other hand, a few works concerning the understanding of the mercury adsorption process on minerals present an electrochemical approach. These works were carried out in acid media and used carbon paste electrodes modified with mineral grains [16,17]. Perdicakis et al. [16] present a comparative study between silver and mercury ions reactivity on pyrite. They concluded that silver ions are almost 20 times more reactive than mercury. Walcarius et al. [17] used silica, goethite and pyrite to evaluate mercury adsorption as a function of pH and chloride concentration. These studies have contributed to the understanding of the mineral/Hg(II) interface, although the identification of the surface species is still open to discussion.

The aim of this work is to study the spontaneous interaction between mercury species and pyrite surface in order to identify which species adsorb on pyrite surface. The nature and the extent of the spontaneous interaction were evaluated using electrochemical techniques.

2. Experimental procedures

A system constituted by a potentiostat/galvanostat AUTOLAB/PGSTAT 20 (Eco Chemie electrochemical instruments), connected to a computer was used to carry out the electrochemical measurements (open circuit potential measurements and cyclic voltammetry).

The electrochemical cell, jacketed and of 100 mL volume, contained an acrylic cell top with a set of holes in order to place the cell components. The working electrode was a carbon paraffin electrode modified with natural pyrite grains. This electrode was constructed according to the Almeida-Giannetti method [18] and consisted of 1.0 g graphite and 1.2 g paraffin containing 5 mg of ground pyrite. The mineral was hand ground in an agate mortar and pestle. This material was then sieved to isolate the fraction containing particles <210 μm in size. The natural pyrite sample is from Morro Velho mine, Minas Gerais, Brazil. Physical and chemical characteristics of the samples are cited elsewhere [19].

The reference electrode was a commercial Ag/AgCl (4 M in KCl) and the counter electrode a platinum platinized wire, both contained in their own compartments. A fritted end of the counter electrode compartment avoids the leaching of products to the working solution.

All the solutions were prepared from treated water obtained from a Milli Q Academic water purifier and analytic grade reagents.

The electrolyte, acetic acid/sodium acetate (0.25 M/0.25 M), pH 4.5 was chosen not only due to its pH value next to that found under weathering conditions [20,21], but also because it acts as a pH buffer and controls the ionic strength of the solution. Moreover, as pyrite behaviour in this working solution was fully investigated [19,37] the influence of mercury presence will be accurately evaluated. Distilled and filtrated metallic mercury and $Hg(NO_3)_2$ 10^{-3} mol L^{-1} and $HgNO_3$ solutions were also used.

Deaeration of the working solution was carried out with ultrapure (99.999%) nitrogen gas.

The voltammograms were performed at a sweep rate of $v = 0.020$ V s^{-1} between the positive and negative potential limits, $E\lambda_a$ and $E\lambda_c$, respectively, indicated in each figure. The scans were always initiated and finished at the open circuit potential value (E_{OC}) of each interface. If scan rate values other than 0.020 V s^{-1} were used, they are indicated in the text. The interaction with Hg(II) ions was carried out by the immersion of the electrode in the $Hg(NO_3)_2$ solution for a time interval indicated in each case. In order to compare results, immersion of the electrode in metallic mercury was also carried out. After immersion, the electrode was carefully washed with treated water and placed into the electrochemical cell. For some specific experiments, $Hg(NO_3)_2$ and $HgNO_3$ salts were added to the working solution to perform the voltammetric measurements.

Working solutions were thermostatized at 25 ± 1 °C. Potentials quoted in this paper were referred to standard hydrogen electrode (SHE).

3. Results and discussion

3.1. Typical potentiodinamic profiles of pyrite

Typical cyclic voltammograms of the pyrite carbon paraffin electrode initiated from E_{OC} towards both positive and negative directions are depicted in Fig. 1. The curves obtained are similar to those presented in literature [19,21].

Equations representing the main reactions associated to the current peaks are listed in Table 1. In the potential window of a_I, the oxidation of mineral surface to form S, SO_4^{2-} and $Fe(OH)_3$

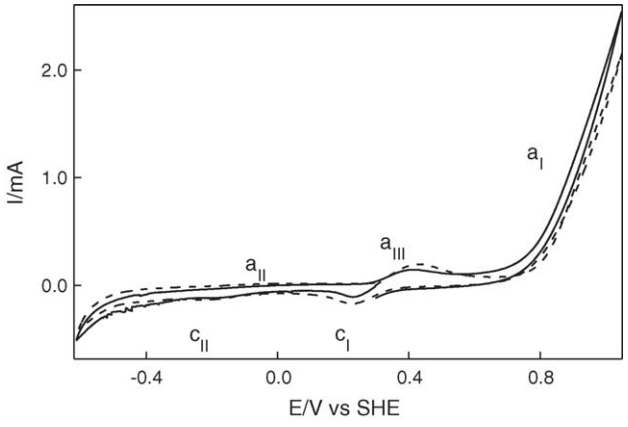

Fig. 1. Cyclic voltammograms of pyrite carbon paraffin electrode in H_3CCOOH/$H_3CCOONa$ buffer solution, started from E_{OC} towards (- - -) positive and (—) negative direction; $E_{OC} = 0.3$ V; $E\lambda_a = 1.0$ V; $E\lambda_c = -0.6$ V, $v = 0.020$ V s^{-1}.

Table 1
Reactions proposed for the main electrochemical processes of pyrite

		Cathodic peak[a]	Anodic peak[a]
$Fe(OH)_3 + 3H^+ + e^- \leftrightarrow Fe^{2+} + 3H_2O$	(1)	c_I	a_{III}
$FeS_2 + 2H^+ + 2e^- \leftrightarrow FeS + H_2S$	(2)	c_{II}	a_{II}
$S + 2H^+ + 2e^- \leftrightarrow H_2S$	(3)	c_{II}	a_{II}
$Fe^{2+} + 2S + 2e^- \leftrightarrow FeS_2$	(4)	c_I	a_I
$Fe^{2+} + 2SO_4{}^{2-} + 16H^+ + 14e^- \leftrightarrow FeS_2 + 8H_2O$	(5)	c_I	a_I

[a] Same simbology of Fig. 1.

occurs according to Hamilton and Woods [22]. The negative going potential scan originates two cathodic peaks c_I and c_{II}. In the potential range of peak c_I, the reduction of $Fe(OH)_3$ produced spontaneously on air and in the course of the previous positive going potential scan occurs (via reaction (1) Table 1). Peak c_{II} is attributed to several reactions, among these, the sulfur reduction (reaction (3)) either electrochemically formed [22] or spontaneously produced during electrode construction. The mineral decomposition yielding H_2S and even H_2 [23,24] is also considered.

The potential scan reversal at $E\lambda_c$ towards positive direction evidences an anodic contribution a_{II}. Thermodynamics predicts the oxidation of the H_2S generated at c_{II} [22] in this potential region. At potentials near 0.4 V a step (a_{III}) is depicted in the current profile. Within this potential domain reaction (1) occurs.

3.2. Mercury ions-pyrite and metallic mercury-pyrite spontaneous interaction

An increase in the open circuit potential value was observed for those electrodes previously immersed in the $Hg(NO_3)_2$ solution. The shift of the E_{OC} towards positive values after the electrode interaction with mercuric ions evidences a more passivated surface. This effect may be explained due to the presence of oxidized species on the surface.

Details of the cathodic and anodic excursions of the voltammogram performed in working solution after 30 min of immersion in Hg(II) containing solution, are depicted in Fig. 2(a) and (b), respectively. Peak c_I is not observed but new current peaks C_1, C_2 and C_3 are recorded in the cathodic profile.

It is possible to identify in Fig. 2(b) peak a_{III}, located in the middle of the new anodic current peaks, A_1, A_2, A_3, A_4 and A_5. Current a_I (not included in the potential interval of the figure) remains practically unaltered after the interaction between pyrite and mercury species. There is no evidence of peak a_{II}. The high number of new processes reflects the complex nature of the pyrite/mercuric ions system. This fact indicates that more than a single species spontaneously forms on the electrode surface and supports the results found in works employing spectroscopic and electrochemical techniques [16,17,25–27].

Peak c_{II} was not systematically observed after the spontaneous interactions between the mineral and the $Hg(NO_3)_2$ solution. But when peak c_{II} is recorded, lower current values of c_{II} compared to those recorded in the absence of Hg(II) interactions are observed.

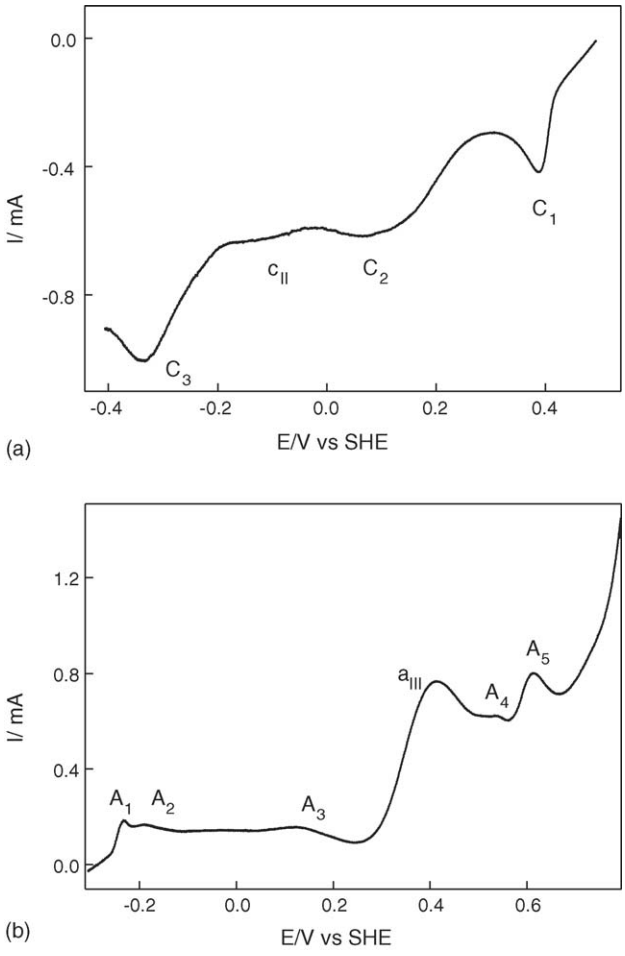

Fig. 2. Cyclic voltammogram of pyrite carbon paraffin electrode in $H_3CCOOH/H_3CCOONa$ buffer solution started from E_{OC} towards the negative direction after interaction with Hg(II) containing solution during 30 min. (a) Detail of the cathodic branch, (b) detail of the anodic branch. $E_{OC} = 0.5$ V; $E\lambda_a = 1.0$ V; $E\lambda_c = -0.6$ V, $\nu = 0.020$ V s^{-1}.

According to Table 1, the current peak c_{II} is attributed to the reduction of the sulfur formed onto pyrite surface or to the reduction of the $S_2{}^{2-}$ species. The lack of reproducibility and the decrease of current values after immersion in $Hg(NO_3)_2$, may be due to the strong interaction between sulfur species and mercury which would partially impede sulfur species reduction. This interference may be justified by the low HgS solubility constant value (2×10^{-52}) [28].

In the work reported by Perdicakis et al. [16], the potentiodynamic profile of pyrite after its interaction with $Hg(NO_3)_2$ solution presents two anodic peaks in the same potential regions of A_4 and A_5 of Fig. 2(b). These peaks were assigned to Hg^0 oxidation process [16]. The elemental mercury would form during the negative going potential scan. Processes A_4 and A_5 are located in the same potential region of the peak assigned to metallic oxidation of a mercury electrode [29]. Perdicakis et al. [16] also describe the presence of two cathodic peaks, each of them related to the reduction of a mercury-containing species [16]. In the present study only the cathodic peak located at 0.1 V, namely C_2, resembles the results obtained by those authors. Differences in electrode construction as well

as in surface pre-treatment can account for the different results mentioned.

Antonijevic et al. [30] studied natural pyrite as an electrochemical sensor for potentiometric titration of Hg(II) and Ag(I) with EDTA. Based on thermodynamic data, they affirmed that Hg(II) ions can react with pyrite according to the following reactions:

$$2Hg^{2+} + FeS_2 \leftrightarrow Hg_2{}^{2+} + Fe^{2+} + 2S^0;$$
$$\Delta G^0 = -93.98\,\text{kJ mol}^{-1} \quad (6)$$

$$Hg^{2+} + FeS_2 \leftrightarrow Hg^0 + Fe^{2+} + 2S^0;$$
$$\Delta G^0 = -83.14\,\text{kJ mol}^{-1} \quad (7)$$

In this way, mercuric ions can be spontaneously reduced either to mercurious ions (reaction (6)) or to elemental mercury on pyrite surface (reaction (7)). Experiments were carried out to evaluate mercury formation on pyrite surface after the immersion in $Hg(NO_3)_2$ 1 mM. Fig. 3 illustrates the voltammograms of the pyrite carbon paraffin electrode recorded at 0.002 V s^{-1}, under two experimental conditions with and without previous $Hg(NO_3)_2$ interaction. The potential sweep was initiated from E_{OC} towards positive direction. From the comparison of the curves in Fig. 3, a surface blockage of pyrite after $Hg(NO_3)_2$ interaction can be inferred. The decrease in peak a_{III} may be attributed to the decrease in the exposed surface as a consequence of the deposition of mercury species. Moreover, its cathodic counterpart disappeared. These results evidence the lesser extent of surface oxidation during positive going potential scan, since the current value measured at the positive potential limit is 20 times greater for the case without interaction with the Hg(II) containing solution.

At potentials more positive than peak a_{III}, two anodic processes A_4 and A_5 are recorded. Similar current peaks were observed by Perdicakis et al. [16], but only when the electrode was negatively swept. The voltammogram detail corresponding to the potential region of the mineral oxidation after interaction with mercuric ions is shown in Fig. 4.

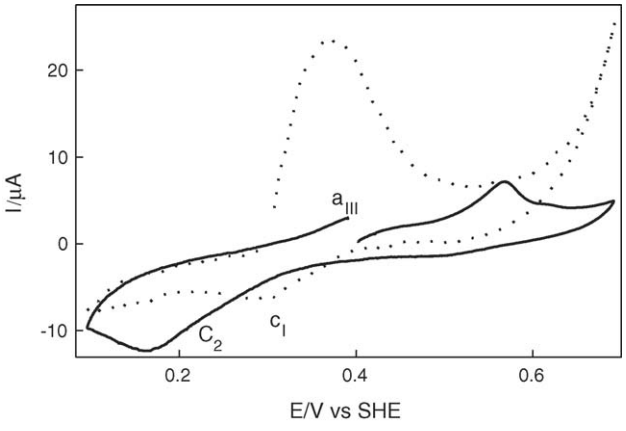

Fig. 3. Cyclic voltammogram of pyrite carbon paraffin electrode in $H_3CCOOH/H_3CCOONa$ quiescent buffer solution initiated from E_{OC} towards positive direction, after interaction with Hg(II) solution during 30 min (—) and without interaction (· · ·); $E\lambda_a$ = 0.7 V; $E\lambda_c$ = 0.1 V, ν = 0.002 V s^{-1}.

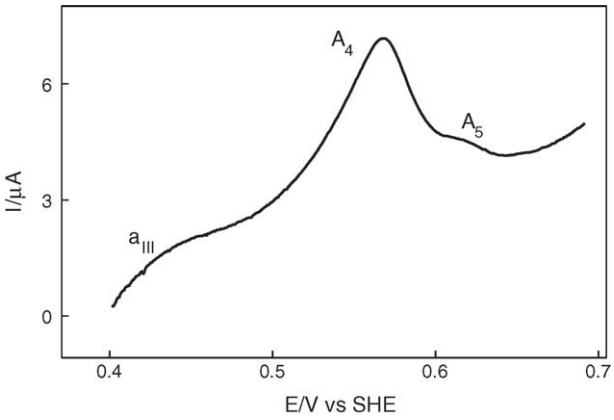

Fig. 4. Detail of the anodic branch of the cyclic voltammogram of pyrite carbon paraffin electrode in $H_3CCOOH/H_3CCOONa$ quiescent buffer solution initiated from E_{OC} towards positive direction, after interaction with Hg(II) solution during 30 min; E_{OC} = 0.4 V; $E\lambda_a$ = 0.7 V; $E\lambda_c$ = 0.1 V, ν = 0.002 V s^{-1}.

The difference between the results obtained by Perdicakis et al. [16] and present study may be attributed to divergences in the experimental conditions. While at Perdicakis et al. [16] pyrite/Hg(II) interaction was carried out for 14 days with constant stirring under inert atmosphere, in the present work interaction was performed during 30 min in aerated quiescent solutions.

The presence of current peaks A_4 and A_5 supports the proposal of the spontaneous reduction of Hg(II) species when kept in contact with the pyrite electrode [30]. In this way, species formed during the spontaneous reduction oxidize in the A_4 and A_5 potential region.

Experiments dealing with the interaction between pyrite and metallic mercury were carried out with two purposes. First, to verify if metallic mercury is retained by the natural pyrite sample, as reported by Brown et al. [13]. Secondly, to compare the electrochemical profiles with those obtained after interaction with Hg(II) ions.

After immersion of the electrode in metallic mercury for 30 min, the open circuit potential measured in the working solution was only 0.020 V greater than that of pyrite. This fact indicates that the deposited species onto pyrite surface after contact with Hg^0 do not attain surface coverage values comparable to those resulting from the contact of pyrite with Hg(II) species.

Fig. 5 presents the voltammograms performed in working solution from E_{OC} towards positive direction, after contact with Hg(II) ions and with metallic mercury. The initial portion of the positive going potential scan shows the current peak a_{III}, supporting the evidence just discussed about the lower surface coverage attained by mercury species after immersion in metallic mercury.

At potentials more positive than peak a_{III}, a broad current contribution located in the same potential region of processes A_4 and A_5 is observed and ascribed to Hg^0 oxidation (the latter deposited during mineral–mercury interaction). Two cathodic processes, C_1 and C_3, located in the same potential region for both cases are displayed when the scan is reversed. Results shown in Fig. 5 verified the retaining ability of pyrite towards mercury ions as well as towards metallic mercury. However, it is

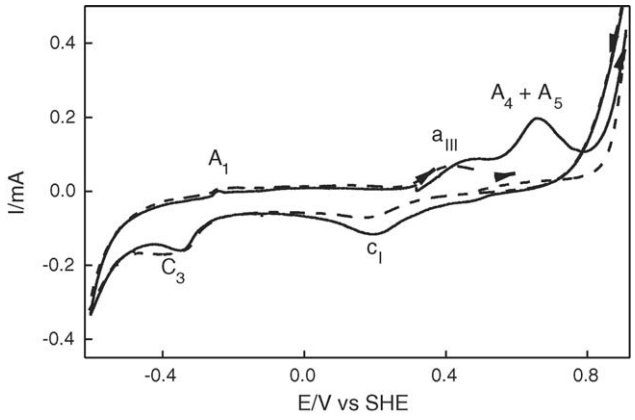

Fig. 5. Cyclic voltammograms of pyrite carbon paraffin electrode in $H_3CCOOH/H_3CCOONa$ quiescent buffer solution initiated from E_{OC} towards the positive direction, after interaction with Hg(II) solution during 30 min (- - -) $E_{OC} = 0.5$ V; and with metallic mercury (—) $E_{OC} = 0.324$ V; $E\lambda_a = 1.0$ V; $E\lambda_c = -0.6$ V, $\nu = 0.020$ V s^{-1}.

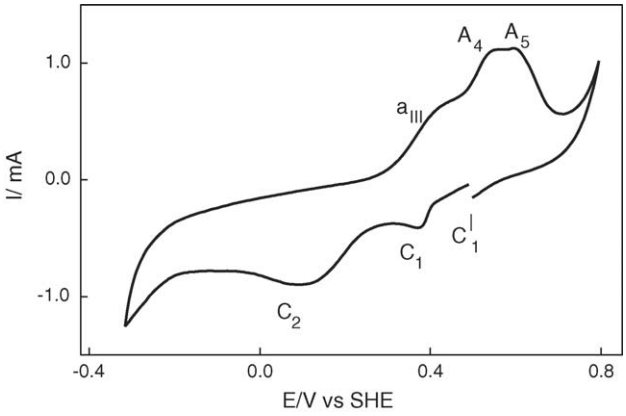

Fig. 7. Cyclic voltammogram of pyrite carbon paraffin electrode in quiescent $H_3CCOOH/H_3CCOONa$ buffer solution initiated from E_{OC} towards the negative direction, after interaction with Hg(II) 1 mM solution during 30 min; $E_{OC} = 0.5$ V; $E\lambda_a = 0.8$ V; $E\lambda_c = -0.3$ V, $\nu = 0.020$ V s^{-1}.

clear that the interaction with Hg(II) solution increases the electrode surface coverage, and consequently a higher impediment towards further surface oxidation is observed.

3.3. Determination of the influence of the negative potential limit on the anodic processes

For determining the potential region in which the species oxidized in A_4 and A_5 are formed after contact with $Hg(NO_3)_2$ solution, a set of voltammograms with fixed $E\lambda_a = 0.8$ V and increasing values of $E\lambda_c$ was performed. This type of experiment allows interpreting the genesis of the anodic processes.

When $E\lambda_c$ was set in -0.4 V (Fig. 6) peaks A_2 and A_3 disappeared from the positive going potential scan. This fact allows inferring that the process occurring at A_2 and A_3 are related to the oxidation of species formed in the potential region more negative than -0.4 V. On the other hand, peaks A_4 and A_5 remain practically unaffected. A little current hump, namely C'_1, was depicted in the negative potential going scan.

When $E\lambda_c = -0.3$ V (value located in the middle of peak C_3), peak A_1 is not depicted in the positive excursion (Fig. 7), indicating that the species oxidized in peak A_1 are generated at potentials more negative than -0.3 V. The relative increase in peak A_4 compared to peak A_5 currents was also observed in the curve.

For values of $E\lambda_c$ selected slightly before the onset of peak C_3, no changes were evidenced at the anodic profile compared with the curve performed under the previously described conditions (Fig. 7). On the other hand, an enhancement of the current hump C'_1 was evidenced in the negative direction.

When $E\lambda_c = 0.28$ V, a value located in the onset of C_2, only peaks A_4 and A_5 appeared in the subsequent positive going potential sweep, being A_5 noticeably diminished (Fig. 8, continuous line). Peaks A_4, A_5 and C_1 are not displayed in the third voltammetric cycle (Fig. 8, dashed line). These experiments clearly show the relation between the processes involved in the cathodic peak C_1 and the anodic processes A_4 and A_5.

Experiments performed in stirring solution were carried out and the results compared with those performed under quiescent

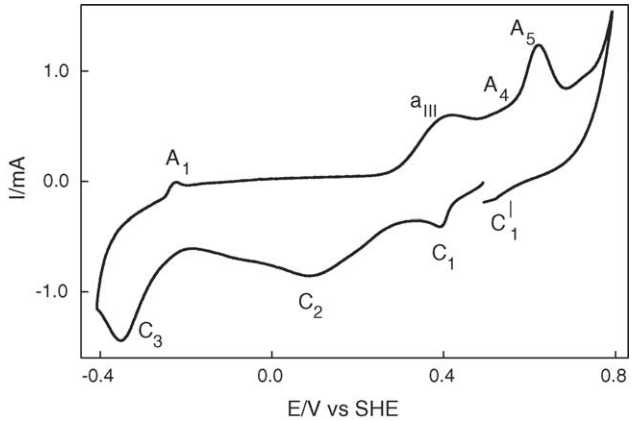

Fig. 6. Cyclic voltammogram of pyrite carbon paraffin electrode in quiescent $H_3CCOOH/H_3CCOONa$ buffer solution initiated from E_{OC} towards the negative direction, after interaction with Hg(II) 1 mM solution during 30 min; $E_{OC} = 0.5$ V; $E\lambda_a = 0.8$ V; $E\lambda_c = -0.4$ V, $\nu = 0.020$ V s^{-1}.

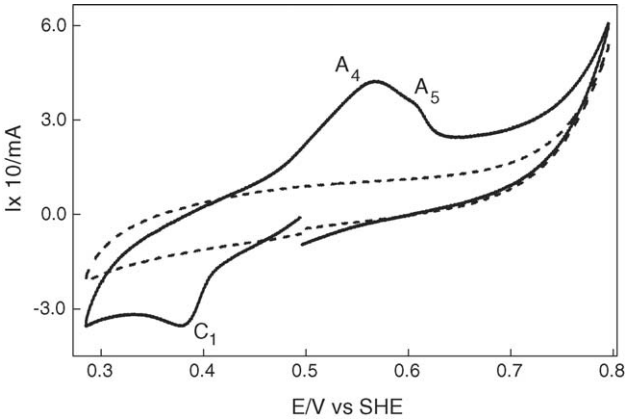

Fig. 8. Cyclic voltammogram of pyrite carbon paraffin electrode in quiescent $H_3CCOOH/H_3CCOONa$ buffer solution initiated from E_{OC} towards the negative direction, after interaction with Hg(II) 1 mM solution during 30 min; $E_{OC} = 0.5$ V; $E\lambda_a = 0.8$ V; $E\lambda_c = 0.28$ V, $\nu = 0.020$ V s^{-1}; (—) first cycle; (- - -) third cycle.

conditions. The decrease of peaks C_1, A_4 and A_5 confirms the soluble nature of the species reduced in the former peak, C_1. When scan was reversed before the onset of peak C_1, no anodic peaks were displayed.

As it was previously observed, peaks A_4 and A_5 current relation changes according to the selected $E\lambda_c$ value. This behaviour supports the hypothesis of the existence of more than a single mercury species on the pyrite surface. These species would be reduced during the negative going potential scan originating peaks A_4 and A_5 when the potential scan is reversed. However, results already shown in this section suggest the existence of another potential region located at more negative potentials than peak C_1 also correlated to processes A_4 and A_5. The hypothesis was explored by means of the following experiment. First, the electrode was subjected to three voltammetric cycles within the 0.29–0.8 V potential interval in order to deplete the soluble species involved in C_1 and that would be oxidized at A_4 and A_5 (Fig. 9, dashed line). Subsequently, a negative going potential scan from the E_{OC} up to $E\lambda_c = -0.4$ V was performed. In this experiment a potentiodynamic profile similar to that presented in Fig. 6 was obtained (continuous line, Fig. 9).

Results shown in Fig. 9 corroborate that more than one species present onto electrode surface can be reduced to Hg^0, resulting in two anodic peaks (peaks A_4 and A_5) when further oxidation is performed. Taking into account the value of the anodic charge density corresponding to these processes (0.34 ± 0.01 mC cm^{-2} from continuous curve of Fig. 9), it can be concluded that peaks A_4 and A_5 are related to the dissolution of a metallic mercury monolayer (0.33 mC cm^{-2}, according to [31]). This monolayer may be formed during processes C_2 and C_3, since species involved in C_1 were depleted during the first three initial cycles.

With the purpose of determining the nature of the species reduced at peak C_1, Hg(II) and Hg(I) ions were individually added to the working solution and voltammograms performed under these conditions. Three cathodic peaks are depicted during the negative scan (Fig. 10) when Hg(I) was added to the solution. Peak C_1, depicted in the initial portion of the scan can

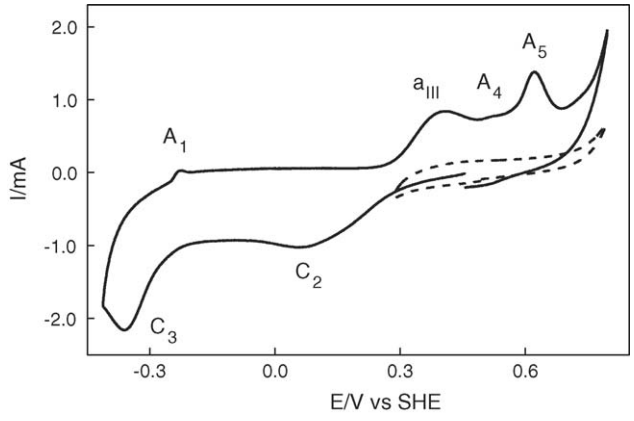

Fig. 9. Cyclic voltammogram of pyrite carbon paraffin electrode in quiescent $H_3CCOOH/H_3CCOONa$ buffer solution initiated from E_{OC} towards the negative direction, after interaction with Hg(II) 1 mM solution during 30 min; $E_{OC} = 0.5$ V; $E\lambda_a = 0.8$ V; (- - -) $E\lambda_c = 0.28$ V; (—) $E\lambda_c = -0.40$ V; $v = 0.020$ V s^{-1}.

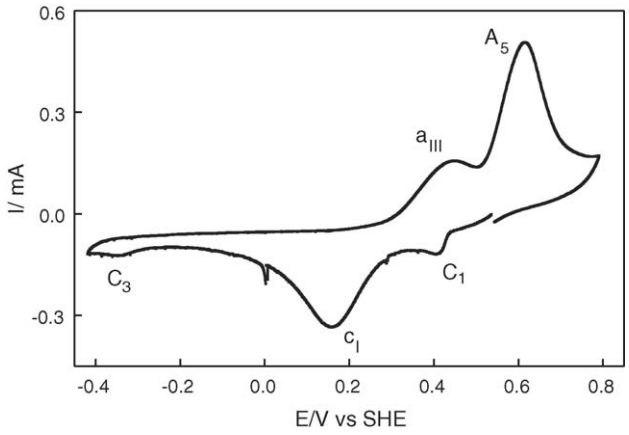

Fig. 10. Cyclic voltammogram of pyrite carbon paraffin electrode in quiescent $H_3CCOOH/H_3CCOONa$ buffer solution added with Hg(I) ions initiated from E_{OC} towards negative direction; $E_{OC} = 0.6$ V; $E\lambda_a = 0.8$ V; $E\lambda_c = -0.40$ V; $v = 0.020$ V s^{-1}.

be associated to Hg (I) reduction to Hg^0 (Eq. (8)) according to thermodynamic data [28]:

$$Hg_{2(aq)}^{2+} + 2e^- \leftrightarrow 2Hg_{(liq)}; \qquad E^0 = 0.796\,V \tag{8}$$

The next peak is located in the potential region corresponding to Fe(III) reduction yielding Fe(II) (process c_I). Process C_3 is also observed. However, in the positive going scan process A_1 is absent. Furthermore, two anodic current peaks are observed at 0.4 and 0.6 V. The first process (a_{III}) is assigned to process c_I counterpart and the second is interpreted as the oxidation process of metallic mercury, formed at C_1. Experiments performed with the addition of Hg(II) into working solution present similar characteristics.

Reaction between Hg(II) and pyrite surface according Antonijevic et al. [30] (Eq. (6)) can account for the similar results obtained in the presence of either Hg(I) or Hg(II) in the working solution. In this way, Hg(II) ions would react with pyrite and generate Hg(I) ions, which would be reduced to Hg^0 in the potential region of peak C_1. This justifies the presence of peak C_1 in both experiments. On the other hand, if the disproportion reaction of Hg(I) is considered, Hg(II) ions could be present in solution after addition of mercurous nitrate:

$$Hg_{2(aq)}^{2+} \leftrightarrow Hg_{(liq)} + Hg_{(aq)}^{2+} \tag{9}$$

Fig. 11 shows voltammograms of pyrite initiated at E_{OC} towards positive direction when Hg(I) and Hg(II) were respectively added to solution. In the case of Hg(II) addition the potential scan was only started after 60 s of electrode immersion in the working solution.

Both curves show peak a_{III} in the beginning of the positive going potential scan. The current peak A_5 at 0.6 V was interpreted as Hg(I) to Hg(II) oxidation. The presence of peaks C_1 and C_1' (attributed to Hg(II) and Hg(I) reduction, respectively) located in the negative going scan after potential reversal, support the interpretation attributed to the anodic peak A_5. This peak was associated with the Hg(I) oxidation in experiments carried out with addition of Hg(II) ions. The Hg(I) species would be spontaneously formed during interaction between pyrite and

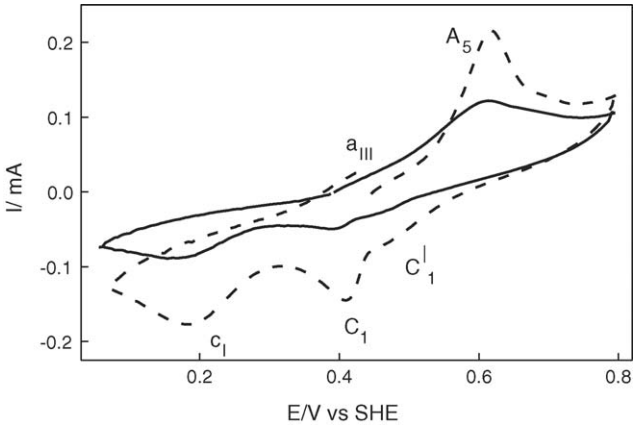

Fig. 11. Cyclic voltammogram of pyrite carbon paraffin electrode in quiescent $H_3CCOOH/H_3CCOONa$ buffer solution initiated from E_{OC} towards the positive direction, with (—) Hg(I) ions: $E_{OC} = 0.4$ V; with (- - -) Hg (II) ions (electrode immersed for 60 s before scan): $E_{OC} = 0.45$ V; $E\lambda_a = 0.8$ V; $E\lambda_c = 0.06$ V; $v = 0.020$ V s^{-1}.

Hg(II) ions, according to Antonijevic et al. [30]. In this way, Hg(I) ions formed during a spontaneous electrochemical step would be oxidized to Hg(II) at peak A_5.

To investigate the formation of Hg(I) ions during interaction between pyrite and Hg(II) ions, the electrode was held at the open circuit potential value for different intervals of time before performing the potential scan. Differently to that observed in Fig. 11, when an interval of 60 s was established before the scan, no anodic processes were observed when the scan was started immediately after electrode immersion. Even so, the reversal of potential scan evidenced current peaks C_1 and C_1'.

Fig. 12 depicts a detail of the initial portion of the positive scan for four different intervals of time. As the time interval increases, the higher is the current recorded for peak A_5. As no anodic current contribution was verified when the sweep was performed immediately after immersion, it may be concluded that greater interaction times with solution lead to an increase of Hg(I) formation.

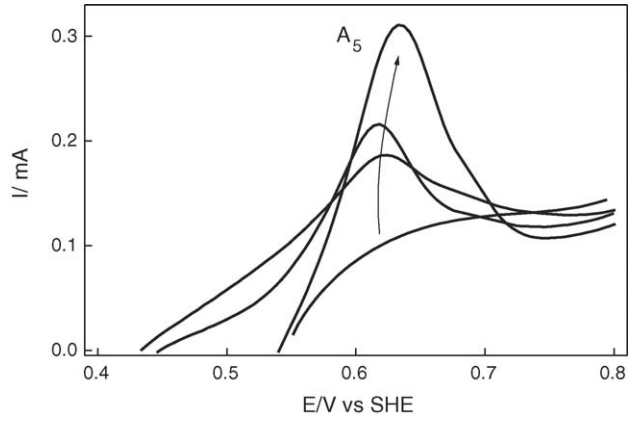

Fig. 12. Detail of the initial portion of the positive scans for pyrite carbon paraffin electrode in $H_3CCOOH/H_3CCOONa$ buffer solution with Hg(II) ions for increasing time intervals between immersion and sweep start; for 0 s, $E_{OC} = 0.55$ V; for 30 s, $E_{OC} = 0.42$ V; for 60 s, $E_{OC} = 0.44$ V; and for 150 s, $E_{OC} = 0.54$ V; $E\lambda_a = 0{,}8$ V; $E\lambda_c = 0{,}06$ V; $v = 0.020$ V s^{-1}.

On the other hand, the complexation model developed for Hg(II) ions adsorption onto oxide and hydroxide surfaces [32–36] and pyrite [27] predicts formation of ternary mercury complexes (≡S−HgOH). The precipitation of $Hg(OH)_2$ onto pyrite is also predicted [27]. In this way, surface species could lixiviate from surface leading to species like $HgOH^+$ [28] (Eq. (10)), being reduced at process C_1.

$$Hg(OH)_{2(aq)} + H_{(aq)}{}^{+} \leftrightarrow Hg(OH)_{(aq)}{}^{+} + H_2O_{(liq)} \quad (10)$$

4. Conclusions

These results represent a first step for the use of mining wastes rich in pyrite, for mercury pollution abatement.

The capacity of retention of mercury ions and metallic mercury by pyrite was verified. Electrochemical experiments carried out after immersion of pyrite in $Hg(NO_3)_2$ solutions showed that mercury species undergo spontaneous reduction on the mineral surface. During the potential scans in the positive direction, it was evidenced that Hg oxidation occurs. The oxidation proceeds in two steps, confirmed by the presence of current peaks A_4 and A_5.

From experiments when negative potential limits were varied, current peaks A_4 and A_5 were associated with the reduction processes occurring at C_1, C_2 and C_3. From these experiments, the relationship between C3 and A1 was also evidenced. Processes A_4 and A_5 are complex in nature, including at least two current contributions: one related to the dissolution of a mercuric monolayer and the other to species in solution.

Acknowledgement

The financial support of this research by FAPESP under project no. 1995/9333-2 is gratefully recognised.

References

[1] J.M. Wood, F.S. Kennedy, C.G. Rosen, Nature 220 (1968) 173.
[2] M. Fujiki, S. Tajima, Water Sci. Technol. 25 (1992) 133.
[3] H. Rustam, Brain 97 (1974) 499.
[4] J. Long, Chem. Eng. News 75 (1997) 11.
[5] B.F. Giannetti, S.H. Bonilla, C.M.V.B. Almeida, J. Cleaner Prod. 12 (2004) 361.
[6] D.G. Kinniburg, M.L. Jackson, J.K. Syers, Soil. Sci. Soc. Am. J. 40 (1976) 796.
[7] L.S. Balistrieri, J.W. Murray, Geochim. Cosmochim. Acta 46 (1982) 1253.
[8] E.A. Forbes, A.M. Posner, J.P. Quirk, J. Soil Sci. 27 (1976) 154.
[9] P. Loganathan, R.G. Burau, Geochim. Cosmochim. Acta 37 (1973) 1277.
[10] H. Farrah, D. Hatton, W.F. Pickering, Chem. Geol. 28 (1980) 55.
[11] T. Hara, T. Endo, K. Ikeda, N. Inaba, Sci. Eng. Rev. Doshisha Univ. 20 (1979) 16.
[12] Y. Baba, N. Matsumura, K. Shiomori, Y. Kawano, Anal. Sci. 14 (1998) 687.
[13] J.R. Brown, G.M. Bancroft, W.S. Fyfe, R.E.N. MacLean, Environ. Sci. Technol. 13 (1979) 1142.
[14] G.E. Jean, G.M. Bancroft, Geochim. Cosmochim. Acta 50 (1986) 1455.
[15] M.M. Hiland, G.E. Jean, G.M. Bancroft, Geochim. Cosmochim. Acta 54 (1990) 1957.
[16] M. Perdicakis, N. Grosselin, J. Bessière, Anal. Chim. Acta 385 (1999) 467.

[17] A. Walcarius, J. Devoy, J. Bessiere, J. Environ. Sci. Technol. 23 (1999) 4278.
[18] C.M.V.B. Almeida, B.F. Giannetti, Electrochem. Comm. 4 (2002) 985.
[19] B.F. Giannetti, S.H. Bonilla, C.F. Zinola, T. Rabóczkay, Hydrometallurgy 60 (2001) 41.
[20] M.O. Schrenk, K.J. Edwards, R.M. Goodman, R.J. Hamers, J. Banfield, Science 279 (1998) 1519.
[21] R.T. Lowson, Chem. Rev. 82 (1982) 461.
[22] C. Hamilton, R.J. Woods, Electroanal. Chem. 118 (1981) 327.
[23] T.J. Biegler, Electrochem. Soc. 70 (1976) 265.
[24] K.A. Radyushikina, V.E. Vidergauz, M.R. Tarasevich, V.A. Chanturiya, Elektrokhimiya 22 (1986) 1394.
[25] J.E. Gilles, M. Bancroft, Geochim. Cosmochim. Acta 50 (1986) 1455.
[26] M.M. Hiland, J.E. Gilles, M. Bancroft, Geochim. Cosmochim. Acta 54 (1990) 1957.
[27] P. Behra, P. Bonnissel-Gissinger, M. Alnot, R. Revel, J.J. Ehrahrdt, Langmuir 17 (2001) 3970.
[28] L.G. Hepler, G. Olofsson, Chem. Rev. 75 (1975) 585.
[29] W.A. Moreira, M.Sc. thesis, Universidade de São Paulo, 2002.
[30] M.M. Antonijevic, R.P. Mihalojlovic, B.V. Vukanovic, J. Solid State Electrochem. 5 (2001) 29.
[31] S.P. Kounaves, J. Buffle, J. Electrochem. Soc. 133 (1986) 2495.
[32] J.R. Bargar, P. Persson, G.E. Brown Jr., J. Phys. IV 7 (1997) C2–C825.
[33] C. Tiffreau, J. Lützenkirchen, P. Behra, J. Colloid Interface Sci. 172 (1995) 82.
[34] P. Bonnissel-Gissinger, M. Alnot, J.J. Ehrhardt, P. Behra, J. Colloid Interface Sci. 215 (1999) 313.
[35] C.R. Collins, D.M. Sherman, K.V. Ragnarsdottir, J. Colloid Interface Sci. 219 (1999) 345.
[36] M. Majone, M.P. Papini, E. Rolle, J. Colloid Interface Sci. 179 (1996) 412.
[37] B.F. Giannetti, C.M.V.B. Almeida, S.H. Bonilla, Colloids Surf. A, doi:10.1016/j.colsurfa.2005.07.018.